AGU PUBLICATIONS

JGR

Journal of Geophysical Research: Atmospheres

RESEARCH ARTICLE
10.1002/2016JD026154

Key Points:
- Stable water isotopes can be used to distinguish between different structures of large-scale vertical velocity
- Top heavy vertical velocity profiles are associated with more depleted precipitation than bottom heavy profiles
- Convection over the eastern Pacific seems more bottom heavy than over the Western Pacific

Correspondence to:
G. Torri,
torri@fas.harvard.edu

Citation:
Torri, G., D. Ma, and Z. Kuang (2017), Stable water isotopes and large-scale vertical motions in the tropics, *J. Geophys. Res. Atmos.*, *122*, doi:10.1002/2016JD026154.

Received 27 OCT 2016
Accepted 2 MAR 2017
Accepted article online 9 MAR 2017

Stable water isotopes and large-scale vertical motions in the tropics

Giuseppe Torri[1], Ding Ma[2], and Zhiming Kuang[1,3]

[1]Department of Earth and Planetary Sciences, Harvard University, Cambridge, Massachusetts, USA, [2]Earth Institute, Columbia University, New York, New York, USA, [3]Harvard John A. Paulson School of Engineering and Applied Sciences, Harvard University, Cambridge, Massachusetts, USA

Abstract A complete understanding of the interaction between convection and the large-scale circulation in the tropics remains an outstanding problem. Although there is evidence that the vertical structure of convective heating has great influence in the large-scale response and that this structure also presents considerable geographical variations, more need to be done. One of the questions that are still unanswered is how the vertical structure of the convective heating, or, similarly, of vertical velocity, varies across the tropical Pacific. Here it is suggested that some light can be shed on this debate by considering stable water isotopes. Because these tend to be progressively less abundant with increasing height, precipitation associated with top heavy profiles should be expected to be more depleted than that associated with bottom heavy profiles. This claim is verified with a variety of data: first, using observations from IAEA/WMO Global Network of Isotopes in Precipitation stations; then, using a simple model based on the budget of water isotopes in precipitation; finally, using a more complex isotope-enabled general circulation model. Evidence provided by these sources confirms that different structures of vertical velocities are associated with different isotopic abundances, with top heavy profiles giving rise to more depleted rainfall. Finally, the data from over the Pacific, although scarce, seem to suggest that precipitation in the eastern part is more enriched than in the western, thus hinting at velocity profiles over the East being more bottom heavy than over the West Pacific.

1. Introduction

How the vertical structure of convective heating varies across the tropics is an important aspect of the large-scale circulation that remains debated. Among the first to highlight the importance of the heating's vertical structure, *Houze* [1982] showed that the net heating produced by mature cloud clusters was more confined and peaked at a greater altitude than the profile associated with a single, isolated convective plume; following that, *Hartmann et al.* [1984] demonstrated that using the former heating profile in a simple atmospheric model [*Hendon and Hartmann*, 1982] gave rise to a significantly more realistic Walker Circulation than was previously obtained with the latter.

Few decades after these studies, it also became clear that the vertical structure also presented considerable geographic variability. Analyzing the first two Empirical Orthogonal Functions of the divergent circulation over the tropics, *Trenberth et al.* [2000] showed that together with the first mode, which is associated with the traditional Hadley- or Walker-like overturning circulations and that can account for 60% of the variance across all seasons, another mode was present that could account for 20% of the variance. This mode was associated with low-level convergence below 800 hPa and a reverse flow at 700 hPa and seemed to be a particularly important component of the overturning circulation in the tropical eastern Pacific and the Atlantic. Although these conclusions had been drawn purely using reanalysis data, they were partially supported by *Zhang et al.* [2004] who, using observations from different sources, showed the existence of a meridional shallow circulation in the tropical eastern Pacific. Another piece of evidence to support the idea that this area of the tropics had a different vertical structure than the more top heavy profile that was usually assumed, and which is more commonly seen in the western part of the Pacific, came from *Back and Bretherton* [2006]. Using three independent reanalysis data sets, their work suggested that the export of Moist Static Energy by vertical and horizontal convergence varies geographically over the tropical Pacific and that this variation is due to differences in the shape of the vertical velocity profile: top heavy in the western Pacific, with mean horizontal

convergence extending up to 300 hPa, and bottom heavy in the eastern part of the basin, with convergence up to 800 hPa and divergence above.

Interestingly, the results briefly discussed above are antithetical to the findings presented in *Schumacher and Kraucunas* [2004], where estimates of vertical profiles of latent heating obtained by the precipitation radar (PR) on board the Tropical Rainfall Measuring Mission (TRMM) [*Simpson et al.*, 1988; *Liu et al.*, 2012] were used to force an idealized version of the Community Climate Model, version 3 (CCM3). The dynamical response provided by the model showed that, indeed, the large-scale vertical velocities showed appreciable geographic differences, but, nonetheless, the profiles of ascent in areas such as the eastern Pacific tended to be top heavy. These findings were recently supported by *Huaman and Takahashi* [2016], using a combination of TRMM PR data and of in situ observations from the Eastern Pacific Investigation of Climate (EPIC2001) [*Cronin et al.*, 2002; *Raymond et al.*, 2004] campaign.

Choosing which side to support in this debate might prove tricky, mainly because the methods used in both cases are not entirely free from criticism. For instance, it could be argued, as *Huaman and Takahashi* [2016] did, that reanalysis products do not fully capture the structure of the Intertropical Convergence Zone (ITCZ) [*Hastenrath*, 2002] or also that reanalyses are known to be affected by potential biases and errors in the radiosonde and satellite data that are used as input [*Mears and Wentz*, 2005; *Santer et al.*, 1999, 2005; *Sherwood et al.*, 2005; *Mitas and Clement*, 2006].

On the observational side, *Back and Bretherton* [2006] pointed out that *Schumacher and Kraucunas* [2004] assumed idealized latent heating profiles that were geographically invariant for their analysis, thus considering only variability associated with differences in the stratiform rain fraction. The results presented by *Schumacher and Kraucunas* [2004] are not very dissimilar to those obtained with other techniques [*Liu et al.*, 2015], though, which could suggest that the assumption of geographical invariance of the idealized latent heating profiles may have not been a critical one. Another potential concern using TRMM PR data, as *Schumacher and Kraucunas* [2004] and *Liu et al.* [2015] did, is that the satellite has a minimum detectable signal of approximately 17 dBZ [see, e.g., *Schumacher and Kraucunas*, 2004; *Lebsock and L'Ecuyer*, 2011; *Liu et al.*, 2015], which hinders its ability to observe weak precipitation as well as nonprecipitating shallow clouds.

To this debate, the presented summary of which we do not hope to be fully exhaustive, we would like to contribute with a novel approach, using a methodology based on stable water isotopes in precipitation. The use of these kinds of techniques to gain a better understanding of atmospheric convection and of the hydrological cycle dates back to *Dansgaard* [1953, 1964], and has been used by many in the following years [see, e.g., *Gedzelman and Lawrence*, 1982; *White and Gedzelman*, 1984; *Jouzel and Merlivat*, 1984; *Kaye*, 1987; *Gedzelman and Arnold*, 1994; *Lee et al.*, 2007; *Bony et al.*, 2008; *Risi et al.*, 2008; *Blossey et al.*, 2010; *Kurita et al.*, 2011; *Moore et al.*, 2014, 2016].

Recently, stable water isotopes were employed in a number of interesting studies. *Bailey et al.* [2015] used them to diagnose convective precipitation efficiency and, through it, discriminate between different circulation patterns. *Aggarwal et al.* [2016] used stable water isotopes to distinguish intense and spatially limited convective rain from widespread, more gentle stratiform rain.

In a similar spirit to the above cited work, here we are interested in answering the following question: can stable water isotopes be used to distinguish top heavy from bottom heavy profiles of large-scale vertical velocity? The basic idea behind the work that we will describe in the rest of the manuscript relies on a budget perspective of precipitation. Let us consider an atmospheric column and assume, for the moment, that we can neglect horizontal advection. Then, in steady state, the amount of water reaching the surface as precipitation is simply given by the water that is evaporated from the surface plus the water vapor that is converged vertically [*Moore et al.*, 2014]. Because the profiles of stable water isotopes are monotonically decreasing with height, for equal surface evaporation rates, different profiles of vertical velocity should be reflected in different isotopic abundances in the precipitation: more top heavy profiles, which converge water vapor over a much deeper layer than bottom heavy profiles, should result in much more depleted rain. In the following, we will develop this idea a bit further, carefully testing the assumptions made and its limitations, and we will apply it to the regions over the tropical oceans.

2. Methods

2.1. Data

In this work, we will use data from a variety of sources. First and foremost, we will consider monthly averages of isotope abundances from the IAEA/WMO Global Network of Isotopes in Precipitation (GNIP) database [see, e.g., *Schotter et al.*, 1996; *Aggarwal et al.*, 2007]. Whereas this network of stations was initially created in 1958 with the goal of detecting atmospheric fallout from nuclear tests, since the 1970s it has been converted to support hydrological studies. Out of all the GNIP stations, we have selected those on islands or near the coasts, having latitude between 15°N and 15°S and at an elevation no greater than 100 m to avoid orographic effects. For reasons that will be clear in the next paragraph, we have further selected only the stations that were active between 1958 and 2002. A full list of the stations used and their main properties is given, in alphabetical order, in Table 1. The stations are also indicated by violet dots on the map shown in Figure 1.

As we will explain in the next subsection, in this manuscript we will classify the monthly isotope abundances according to the average bottom heaviness and magnitude of the profiles of large-scale velocity for each station. Because the GNIP data set does not provide enough information for this kind of grouping, we will consider data from the European Center for Medium-Range Weather Forecasts 40 year reanalysis (ERA-40) data set [*Simmons and Gibson*, 2000]. Notice that the reanalysis spans a time period between September 1957 and August 2002, thus matching the temporal window we are using to sample GNIP data. From the reanalysis, we will use the monthly averages of pressure velocity, water vapor specific humidity, absolute temperature and the surface latent heat fluxes.

Finally, in order to check the results obtained from observational data, we will use two numerical models. The first one is the isotope-enabled System for Atmospheric Modeling [*Khairoutdinov and Randall*, 2003], version 6.8.2, that we will refer to as *IsoSAM*. The model solves the anelastic equations of motion and uses liquid water static energy, and the mass mixing ratios of various microphysical species, depending on the microphysics scheme used, as thermodynamic prognostic variables. The equations are solved with doubly periodic boundary conditions in the horizontal directions. A prognostic turbulent kinetic energy 1.5-order closure scheme is used to parameterize subgrid scale effects. The surface fluxes are computed using the Monin-Obukhov similarity theory.

We will use the Lin microphysics scheme, a single-moment scheme that incorporates mass mixing ratios of water vapor, cloud liquid water, cloud ice, rain, snow, and graupel [*Lin et al.*, 1983; *Blossey et al.*, 2010]. IsoSAM contains the heavy water isotopologues, HDO and $H_2^{18}O$, which are subject to the same transformation processes as the lighter isotopologue, $H_2^{16}O$. For details on how fractionation is incorporated in the model, we refer the reader to the Appendix B of *Blossey et al.* [2010].

We run the model using the same configuration as in *Moore et al.* [2014]: we set the sea surface temperature (SST) at 301.15 K and run the model for 120 days on a domain that measures 128×128 km^2, and 64 vertical levels reaching an altitude of 32 km, using a stretched grid. The horizontal resolution is 2 km and the temporal resolution is 30 s. We run the model without imposing the weak temperature gradient approximation or prescribing any large-scale vertical velocity. In this work, we will be interested in the average vertical profiles of the stable water isotopes, which we diagnose directly from IsoSAM considering the last 40 days of simulation.

The beauty in the simplicity of using IsoSAM has to be paid with some limitations: the contribution of horizontal advection cannot really be accounted for. In order to achieve this, we consider an isotope-enabled version of the Community Atmospheric Model, version 5 [*Neale et al.*, 2010], or CAM5, the atmospheric component of the NCAR Community Earth System Model [*Hurrell et al.*, 2013]. We will refer to this model as *iCAM5* [*Konecky et al.*, 2014; *Nusbaumer et al.*, 2014; *Nusbaumer*, 2016].

The model runs using a finite-volume dynamical core, and with a horizontal resolution of 1.9 latitudinal and 2.5 longitudinal degrees. In the vertical direction, it has 30 layers that go from the surface to a pressure height of 3 hPa with a stretched grid. At the surface, the model is coupled with iCLM4 and iCICE4, respectively an isotope-enabled land and sea ice models. Initial conditions and forcings for all the components are the same as those described in *O'Brien et al.* [2016]. The isotopic composition of water vapor evaporated from the ocean surface is assumed constant in time and with a spatial distribution given by the data set of *LeGrande and Schmidt* [2006]. We spun up the iCAM5 for 1 year then collected data every 6 h of model time for the following 10 years.

Table 1. List of GNIP Stations Used in This Manuscript Complete With Their Main Properties

WMO Code	Location	Latitude (°N)	Longitude (°E)	Altitude (m)
4860300	Alor Setar	6.2	100.4	5
9176200	Apia	−13.8	188.2	2
6190000	Ascension Island	−7.9	345.6	15
7895400	Barbados (Seawell Airport)	13.1	300.5	50
8002800	Barranquilla	10.9	285.2	14
4343600	Batticaloa	7.8	81.8	5
8219101	Belem Piracicaba	−1.5	311.5	24
9170000	Canton Island	−2.8	188.2	2
9149000	Christmas Island	2.0	202.5	3
4346600	Colombo	6.9	79.9	7
9412000	Darwin	−12.4	130.9	26
6196700	Diego Garcia Island	−7.3	72.4	1
8401800	Esmeraldas	1.0	280.4	30
8239700	Fortaleza	−3.8	321.4	27
7877201	Golfito	8.7	276.8	15
4349700	Hambantota	6.1	81.1	20
7876002	Herradura	9.7	275.4	3
7880600	Howard Air Force Base	8.9	280.4	13
9674500	Jakarta	−6.2	106.8	8
9769800	Jayapura	−2.5	140.7	3
4855000	Ko Samui	9.5	100.1	7
4846000	Ko Sichang	13.2	100.8	26
4861500	Kota Bahru	6.2	102.3	7
4331400	Kozhikode	11.2	75.8	20
4861800	Kuala Terengganu	5.4	103.1	10
4860000	Langkawi	6.3	99.7	31
8424800	Machala	−3.2	280	6
9401400	Madang	−5.2	145.8	4
7875502	Nosara	10.0	274.3	15
4864702	Olak Lempit	2.8	101.6	13
7877200	Palmar Sur	9.0	276.5	16
7876000	Puntarenas	10.0	275.2	3
8322900	Salvador	−13	321.5	45
9161000	Tarawa	1.3	172.9	4
9674502	Tongkol	−6.1	106.8	10
9133400	Truk	7.5	151.9	2
4346601	Wellampitiya	7.0	79.9	5
9141300	Yap	9.5	138.1	23

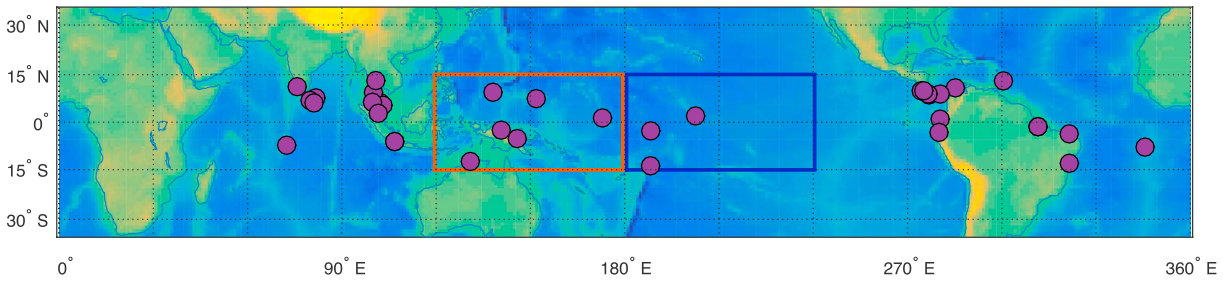

Figure 1. Portion of projected world map showing the GNIP stations used in this study. The orange and the blue rectangles encircle what we define in this manuscript as West (15°N–15°S; 120°E–180°E) and East Pacific (15°N–15°S; 180°E–240°E), respectively.

2.2. Tools and Definitions

Before looking at the results, we must decide how the data will be presented to answer the question outlined in section 1. The main quantity that we will be interested in is the abundance of heavy isotopes in precipitation. For simplicity, we will concentrate on deuterium, ^{2}H or D, but a similar analysis with ^{18}O could also be carried out leading to similar conclusions.

Following the standard convention, we will measure the abundance of deuterium with the following formula:

$$\delta D = \left(\frac{R_{\text{sample}}}{R_{\text{VSMOW}}} - 1 \right) \cdot 1000‰, \tag{1}$$

where R_{sample} is the ratio of deuterium to the common, stable isotope of hydrogen — sometimes called *protium* — in the sampled considered, and R_{VSMOW} is the same ratio but for a reference sample with the isotopic composition of the Vienna standard mean ocean water.

Given the question that we are interested in, we want to be able to group measures of deuterium abundance in the rain according to the shape of the vertical velocity associated with a particular precipitation rate. For this reason, we define a bottom-heaviness index, p_ω, as the pressure velocity-weighted average pressure:

$$p_\omega = \frac{1}{N} \int_{p_s}^{p_t} p\omega \, \mathrm{d}p, \tag{2}$$

where $N = \int_{p_s}^{p_t} \omega \, \mathrm{d}p$ is a normalization factor and the integrals are taken from the surface pressure, p_s, up to the pressure at the top of the troposphere, p_t. Notice that, as mentioned in section 1, the data from the GNIP stations that we are planning to use do not contain information about the pressure velocity profiles for each month of observed isotopes abundances. In order to obviate this problem, we will consider profiles from ERA-40 reanalysis.

In grouping the isotope abundances, there is another variable that we have to take into account. In fact, it is well acknowledged that, especially in the tropics, the isotopic composition of rainfall is susceptible to the so-called *amount effect* [see, e.g., *Dansgaard*, 1964; *Rozanski et al.*, 1993; *Bony et al.*, 2008; *Risi et al.*, 2008; *Moore et al.*, 2014]: large rainfall rates tend to give rise to more depleted precipitation than smaller rates do. There follows that the precipitation rate has to be properly accounted for when arranging the data. Because we want to be as consistent as possible with the reanalysis data that we are using to provide the measure of the velocity's bottom heaviness described above, the most straightforward approach here would probably be to use the precipitation rates in the reanalysis. However, it is well known that these quantities are particularly problematic [see, e.g., *Bosilovich et al.*, 2008] and should not, in general, be completely trusted. Thus, we choose to use another index, that we will call C/E, given by the ratio between the water vapor that is vertically converged and that which is evaporated from the surface through latent heat fluxes:

$$C/E = -\frac{1}{\rho_w \overline{q_v' \mathbf{v}'}} \int_{p_s}^{p_t} q_v \frac{\partial \omega}{\partial p} \frac{\mathrm{d}p}{g}. \tag{3}$$

where ρ_w is the density of liquid water, and $\overline{q_v' \mathbf{v}'}$ represents the turbulent water vapor fluxes at the surface. Notice that, if one considers the budget of water vapor in a column of atmosphere, vertical convergence and surface evaporation are not enough to compute precipitation rates: horizontal advection should also be accounted for. Nevertheless, we found that including horizontal advection in our analysis by using P/E as a variable did not change our conclusions. Throughout this manuscript, we will group data in C/E bins of size 1, and, for simplicity, we will refer to each bin by the initial value of the interval it covers. For example, when we will refer to profiles with C/E equal to 2, the reader should understand all the profiles with a ratio between 2 and 3. Just to provide some physical intuition, this ratio corresponds roughly to a rain rate of 8–10 mm d^{-1}.

Before continuing, we want to verify that our definitions lead to a sensible classification of the data. In particular, we need to check that pressure velocity profiles with higher p_ω correspond to profiles that are more bottom heavy than those with a smaller p_ω. Figure 2 (left) shows a collection of pressure velocities with different values of p_ω for a C/E equal to 2. Each profile is the average of profiles within the same p_ω bin measuring 25 hPa, taken over all the oceanic grid boxes with latitude between 15°N and 15°S and for all the duration of the reanalysis data set. The colors indicate increasingly higher values of p_ω, with the darkest blue corresponding to a value of 400 hPa, and the brightest yellow corresponding to 800 hPa. Figure 2 (right) shows the density

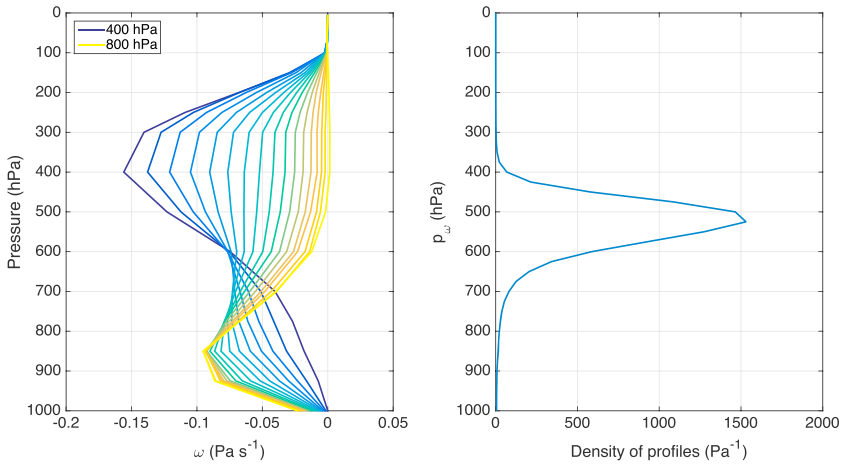

Figure 2. (left) Collection of pressure velocity profiles with increasingly higher (from blue to yellow) p_ω, and $C/E = 2$ averaged over all the oceanic grid boxes between 15°N and 15°S of latitude and over the length of the reanalysis data set. (right) Density of pressure velocity profiles as a function of p_ω. See the text for further information.

of profiles as a function of p_ω. Notice that 95% of all the profiles has a p_ω between 350 and 650 hPa. That this should not be surprising could be understood with a very simple model. Let us approximate the shape of a generic pressure velocity profile by a piecewise linear function. Let us also assume that the function vanishes at the pressure top and surface, indicated, respectively, p_t and p_s, and that its minimum value is attained at pressure height p_h and equal to Ω. The only linear function that obeys these constraints is given by

$$\omega(p) = \begin{cases} \Omega\left(\frac{p-p_t}{p_h-p_t}\right) & \text{if } p < p_h \\ \Omega\left(\frac{p-p_s}{p_h-p_s}\right) & \text{if } p \geq p_h \end{cases} \tag{4}$$

With the definition given in equation (2) and a little bit of algebra, it is easy to prove that

$$p_\omega = \frac{1}{2}\left(\frac{p_h^2 - \frac{1}{3}\left(p_t^2 + p_s p_t + p_s^2\right)}{p_h - \frac{1}{2}\left(p_t + p_s\right)}\right). \tag{5}$$

By construction, the smallest and the greatest values for p_ω can be achieved when $p_h = p_t$ and $p_h = p_s$, respectively. If, for simplicity, we assume that p_s equals 1000 hPa and p_t is 0 hPa, then p_ω is constrained to lie within the range of $333.\overline{3}$ and $666.\overline{6}$ hPa. Notice that Figure 2 (right) suggests the presence of vertical profiles with p_ω beyond the derived bounds. This apparent contradiction can be explained by reminding the reader that we obtained the bounds by assuming the profiles to be piecewise linear. Figure 2 (left) should show convincingly enough that this approximation does not hold in reality, and, therefore, the bounds should be taken more as guiding lines for where most of the profiles should be found.

Another interesting thing to examine is the spatial variability of p_ω, as this will give us some idea on which areas in the tropics should be expected to have a more bottom heavy profile, at least according to the reanalysis. In order to do this, we consider the ERA-40 data set, examine the grid boxes over the ocean with latitude between 15°N and 15°S, and simply average together the p_ω associated with vertical velocity profiles whose ratio of vertically converged over evaporated water vapor is in the same bin. The results for $C/E = 2$ can be seen in Figure 3. One of the first features that jumps to the eye is the large area over the eastern Pacific with average pressure velocity profiles that are much more bottom heavy than the western part of the basin. This is consistent with Figure 4 of *Back and Bretherton* [2006], which shows average pressure velocity profiles derived from the same reanalysis data as the one used here for two areas in the tropical Pacific for different precipitation rates. There also does seem to be some consistency with Figures 5 and 6 presented in *Trenberth et al.* [2000], particularly with respect to the eastern part of both the Pacific and the Atlantic Ocean, and the southern part of the Indian Ocean. Finally, notice that the white areas in the southern tropical Atlantic and southeastern tropical Pacific contain missing values, meaning that for no month in the 40 year span of the data set does vertical convergence of water vapor ever become particularly strong. On the other hand,

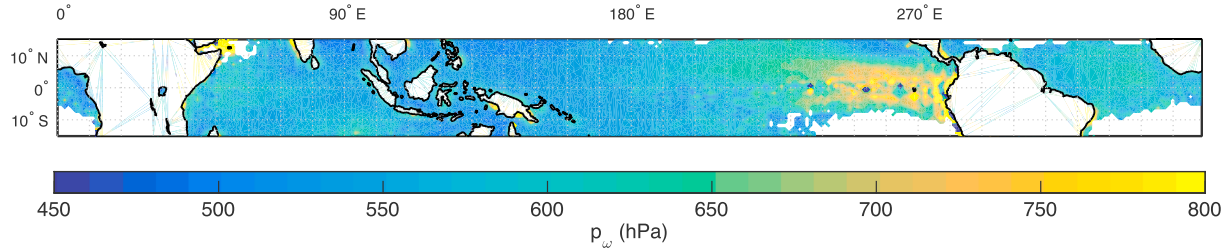

Figure 3. Spatial distribution of p_ω averaged over all the values obtained from all pressure velocities having $C/E = 2$ in grid boxes over the tropical oceans.

this should not be too surprising: comparison with *Trenberth et al.* [2000], for example, suggests these are typically areas of large-scale descent.

3. Results

3.1. The GNIP Data

In order to present the data obtained from the GNIP stations, we consider all the measurements and bin them according to their associated p_ω and C/E ratio, introduced in the previous section, with bin sizes 25 hPa and 1, respectively. Then, we average together values in the same bin and plot the results in Figure 4 (left); Figure 4 (right) shows the number of measurements for each $(p_\omega, C/E)$ couplet.

Although the data are rather noisy, there seem to be two messages emerging from this plot. The first is, as expected from *Lee et al.* [2007] and *Moore et al.* [2014], that precipitation becomes progressively more depleted for increasing C/E ratio. Remembering that this variable is directly related to the precipitation rate, this is simply a restatement of the widely acknowledged amount effect. The second lesson that emerges is that, for a fixed value of C/E, precipitation becomes more depleted for decreasing p_ω, or, otherwise stated, for progressively more top heavy velocity profiles. As we mentioned in section 1, the vertical profile of HDO tends to be monotonically decreasing with height. Because a top heavy profile converges air from a deeper atmospheric layer, the water vapor itself will on average be more depleted than if the air were converged from a shallower layer near the surface.

One way to check whether we are being deceived by our eyes and no significant trends are actually there in Figure 4 is to fit the data with a linear model of the type:

$$\delta D \sim \delta D_0 + a_1(C/E) + a_2(p_\omega) + \epsilon, \tag{6}$$

The choice of using a linear model is mostly dictated by the desire for simplicity: a priori, there is no reason to believe that δD should scale linearly either with p_ω or C/E. This could certainly be a hazardous assumption if we were trying to exactly quantify this dependence. However, since we are only testing the consistency of our

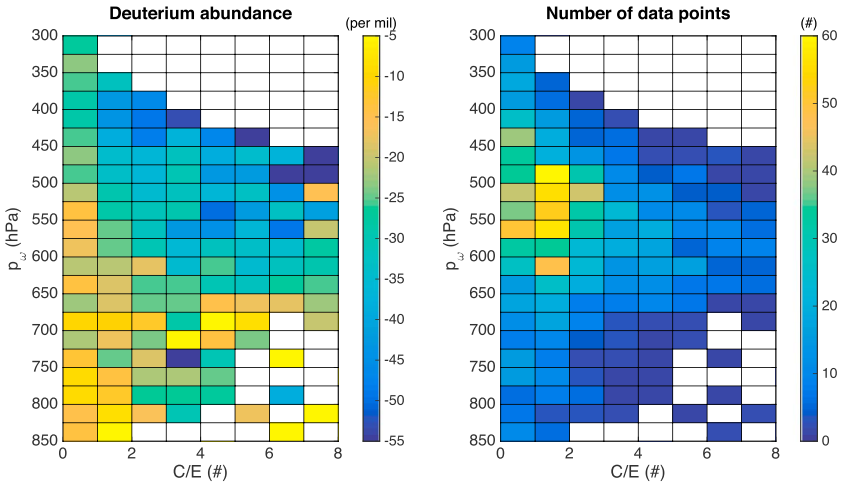

Figure 4. (left) Average δD for various p_ω and C/E obtained from the GNIP data; (right) number of measurements used to compute the averages shown in the other panel.

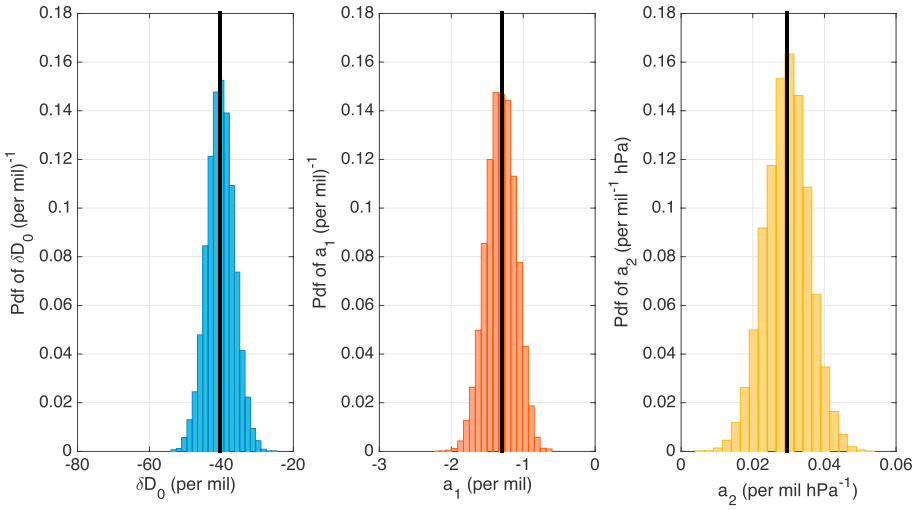

Figure 5. Probability distribution functions for (left) δD_0, (middle) a_1, and (right) a_2 coefficients for the linear model of equation (6), computed using 10,000 bootstrap samples of the GNIP data. The coefficients relative to the fit of the GNIP data set are shown by thick, black vertical lines.

claims, we believe that a linear model like the one shown above will be sufficient. Through a linear regression on the GNIP data, we estimate that δD_0 equals −40.33‰, a_1 is −1.29‰, and a_2 is equal to $2.96 \cdot 10^{-2}$ ° hPa^{-1}. To assess the significance of these coefficients, we create 10,000 bootstrap samples from the original data set, repeat the linear fit for each of them, and create a probability distribution function for each coefficient. Notice that the linear regressions are weighted using the standard deviation of δD computed from the bootstrap samples. The results of this procedure are shown in Figure 5, with the thick vertical bars representing the values for the original GNIP data. Using the width of the distribution as a measure of the uncertainty associated with each coefficient, our results suggest that the trends we spotted in Figure 4 are robust.

3.2. A Consistency Check With IsoSAM

Another way to verify that precipitation associated with bottom heavy velocity profiles is less depleted than that with more top heavy profiles is by using IsoSAM, the isotope-enabled cloud-resolving model introduced in section 2. The idea that we want to pursue is that, if we assume a budget perspective, neglecting horizontal advection for a moment, the amount of water vapor or any heavy water isotope in precipitation is given by the sum of the contribution from surface evaporation and that from the vertical convergence [*Moore et al.*, 2014]. There follows that the ratio of deuterium to the lighter water isotope in the rain at the surface is given by:

$$R_{\text{sample}} = \frac{C_D + E_D}{C_H + E_H}, \tag{7}$$

where E_x are the evaporation fluxes and $C_x = \int q_x \frac{\partial \omega}{\partial p} \frac{dp}{g}$ is the amount of precipitation of a certain isotope given by vertical convergence. We can now compute this ratio—and, therefore, the deuterium abundance—explicitly by using the pressure velocities given by the reanalysis and extracting the vertical profiles of water vapor and HDO specific humidities, along with their surface evaporative fluxes, from IsoSAM. The results of this procedure are shown in Figure 6.

There are two features worth being discussed now. First of all, the two trends that were highlighted in the previous section looking at the GNIP data are clearly visible, also thanks to the smoothness of the results. For example, if we consider the profiles with C/E equal to 2, the range of δD spans an interval of roughly 60‰. The second thing that we want to note is that, for any value of C/E or p_ω, precipitation seems more depleted than what we saw with the GNIP data set. This is not surprising if we consider the vertical profile of δD in IsoSAM, represented by the blue curve in Figure 7. We believe that this is not due to any error on our part, especially given that, as the other curves in the figure suggest, other studies that have used numerical models [*Bony et al.*, 2008; *Kurita et al.*, 2011] have also observed very depleted water vapor at all heights. Rather, as also noted by *Bony et al.* [2008], we suggest that the very depleted precipitation in IsoSAM is the result of neglecting horizontal advection: in fact, the latter could potentially provide a significant inflow of air that,

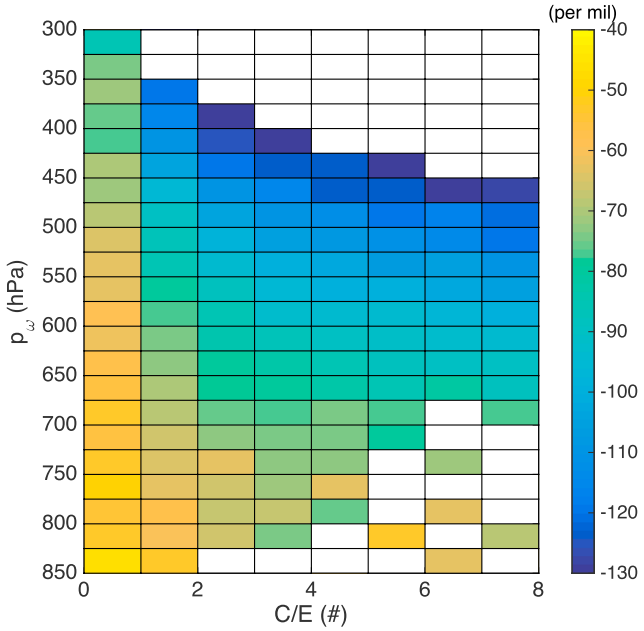

Figure 6. Same as in Figure 4 (left) but estimating δD of precipitation using IsoSAM and neglecting horizontal advection.

not having experienced any effects due to condensation or evaporation of water, is more enriched and which could, in turn, result in less depleted precipitation.

3.3. A Comparison With ICAM5

The main advantage of IsoSAM is its simplicity: simulating an isolated column of atmosphere in radiative-convective equilibrium allows us to study convective processes at relatively fine resolution without the interference of the large-scale. In this case, however, the lack of interaction with the surroundings might have biased low our estimate for the δD of precipitation. Furthermore, the profiles of vertical velocity used in

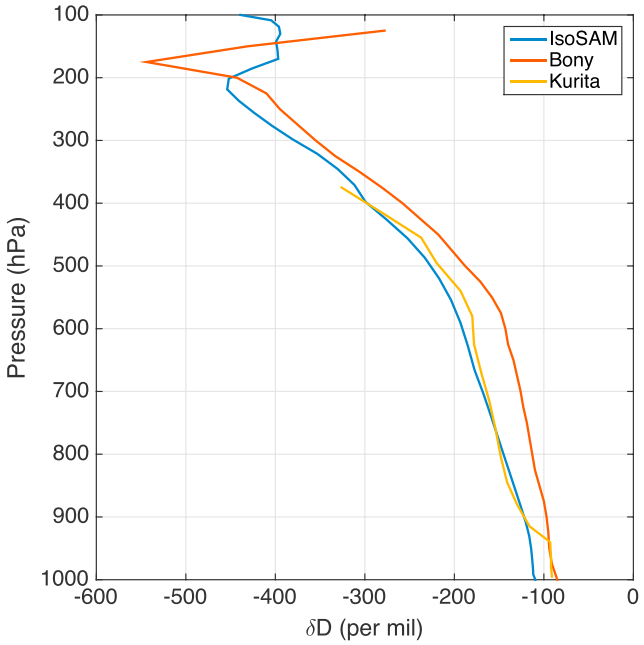

Figure 7. Comparison between the vertical δD profile diagnosed from IsoSAM and those given by *Bony et al.* [2008] in their Figure 6 (black lines) and *Kurita et al.* [2011] in their Figure 8 (green line).

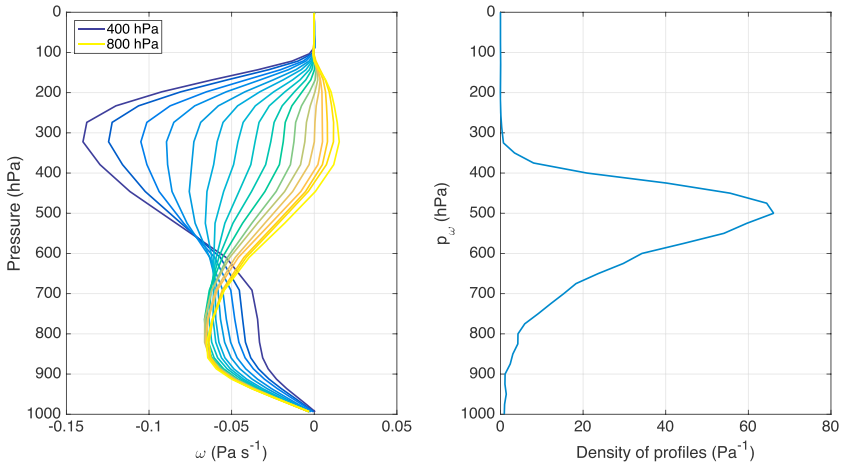

Figure 8. Same as in Figure 2 but using pressure velocities derived from iCAM5.

Figure 6 are not really derived from IsoSAM itself, but are taken from the ERA-40 reanalysis. To assess the role of horizontal advection and to have a self-consistent analysis, we turn our attention to iCAM5.

First of all, to ensure that the variables that we have used so far are still effective, we want to look at pressure velocities for different values of p_ω. Figure 8 is constructed much in the same way as Figure 2, but using data from iCAM5, instead. The top heavy profiles are fairly similar in the two cases, although the pressure height where the minimum ω occurs for iCAM5 profiles is approximately 100 hPa lower than the reanalysis; the more bottom heavy profiles (in orange and yellow colors) are slightly less negative and present a divergence that extends toward greater altitudes than did the profiles from the reanalysis. This having been said, we should note that the differences are fairly small, which gives confidence on the applicability of the metrics used so far on the iCAM5 data.

Then, we essentially repeat the same analysis we have carried out on the GNIP data, but using the surface values of precipitation and pressure velocities from the model. Also, because we do not have to limit ourselves to some specific locations, we will sample all the grid boxes over the ocean and in a latitudinal band between 15°N and 15°S. Figure 9 (left) shows the values of δD in surface rainfall diagnosed from the model as a function of p_ω and C/E, whereas Figure 9 (right) shows values of δD estimated assuming precipitation is given by the sum of the condensate derived from vertical convergence and surface evaporation. The figures suggest that the model confirms our previous finding that rainfall for a given C/E ratio becomes more depleted with

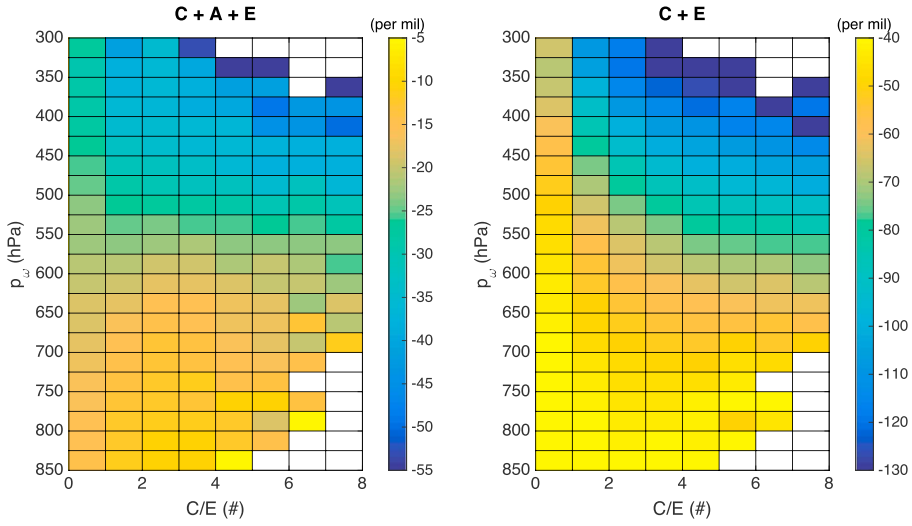

Figure 9. (left) Same as in Figure 4 (left) but using pressure velocity and δD in precipitation from iCAM5; (right) values of δD computed using equation (7), without taking horizontal advection into account.

progressively more top heavy pressure velocity profiles. Interestingly, the dependance of δD on p_ω seems much stronger compared to that with respect to C/E.

Figure 9 (right) also suggests that the bias observed in Figure 6 is likely to be attributed to neglecting horizontal advection. Finally, notice also that comparing the two panels with Figures 4 and 6, respectively, one can see a good agreement, not only for the trends in both directions of the plots but also on the range of variations of δD, which are almost the same as those observed with GNIP data.

4. Discussion

In the previous section, we have presented, from the observations and the models, some evidence that, for a given precipitation rate, bottom heavy vertical velocity profiles tend to give rise to more enriched precipitation than the top heavy ones. Given this result and the premise discussed in section 1, one cannot help but wonder whether stable water isotopes could be used to infer something about the large-scale convective environment in the tropical Pacific Ocean. We will approach this task using the data from the GNIP network of stations.

To begin with, we consider the initial list of stations and we sample those in the Pacific Ocean that are far from continental areas. We further divide the stations in two regions, east and west, using the 180°E meridian as the dividing line. Although this is a rather arbitrary choice, we believe that it is not tremendously out of place, particularly given the speculative nature of this analysis. In order to have a clear visualization of these areas, we invite the reader to look at Figure 1. With the choices made, we are left with the following stations: Darwin, Jayapura, Madang, Tarawa, Truk, and Yap in the west; and Apia, Canton Island, and Christmas Island in the east. The number is certainly not sufficient to draw robust conclusions, but we deem it satisfactory for the present discussion.

For every station, we collect all the monthly means of δD in precipitation and the associated precipitation rate. To prevent the noise from complicating the reading of the results, we have grouped data into five categories according to the precipitation rate: 0–5, 5–10, 10–15, 15–20, and 20–25 mm day^{-1}. Within each category, we compute the average δD for the two different parts of the basin and the associated errors. The results are presented in Figure 10.

Results for each part of the ocean considered separately are just the manifestation of the well-known amount effect. The values of δD for precipitation rates higher than 20 mm d^{-1} in the western area are actually more enriched than those for lower precipitation rates. A closer look at the data suggests that, for high rain rates, most of the values come from the GNIP station at Darwin, situated in the Northern Territory of Australia. Precipitation sampled in this place seems actually less depleted than that in other stations in the West Pacific for all values of precipitation rate. Comparing Darwin's geographical location with that of other stations we are considering, we cannot exclude that the presence of a vast land surface near the station could bias the isotopic composition of rainfall. Moreover, for rain rates higher than 20 mm d^{-1}, there are only 19 measurements in the west and three in the East Pacific, numbers that are roughly an order of magnitude smaller than those for lower rain rates. Results in this interval should, therefore, be taken with caution.

In spite of the behavior at the highest rain rates, the comparison between the values relative to the west and the East Pacific suggests that, indeed, precipitation tends to be more depleted in the former area. Considered under the light of the results presented in the previous section, this could be interpreted as evidence supporting the presence of more bottom heavy velocity profiles in the East Pacific compared to the west.

Because we have argued and showed in the previous sections that horizontal advection also has an effect on the deuterium abundance of precipitation, there is the possibility that the differences we are observing in Figure 10 between West and East Pacific could be ascribed entirely to differences in horizontal advection between the two parts of the basin. In order to check whether this is the case, we consider again the output from iCAM5. First, as illustrated in Figure 1, we divide the Pacific Ocean into two rectangles: 15°N–15°S and 120°E–180°E for the west, and 15°N–15°S and 180°E–240°E for the east. Trying different other choices for these domains, we verified that our conclusions are not sensitive to the precise definition employed here.

The leftmost panel of Figure 11 shows the δD in precipitation diagnosed from iCAM5 binned with the same criteria and the same color choices as Figure 10: at a qualitative level, the comparison between the two figures

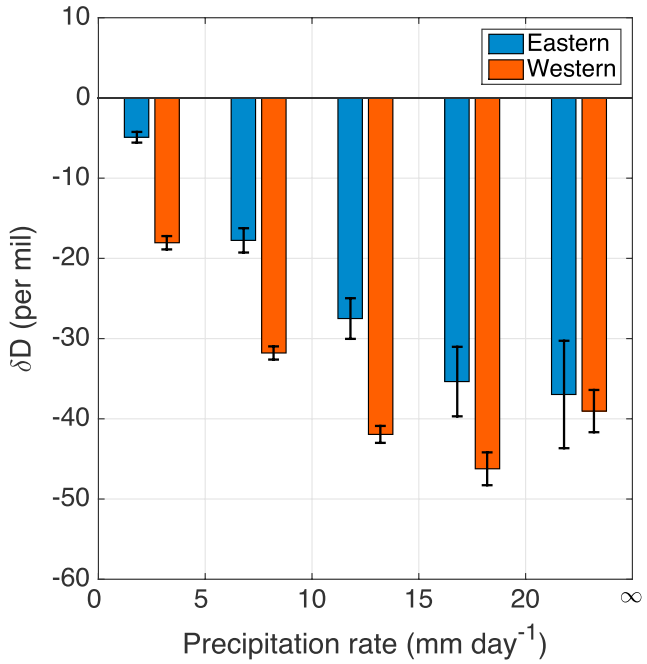

Figure 10. Average deuterium abundance in precipitation for different intervals of monthly averaged precipitation rates as diagnosed entirely using data from GNIP stations. The orange bars refer to results in the West Pacific, the blue ones to those in the East.

is satisfactory. The second panel from the left in Figure 11 represents δD_{rec}, the deuterium abundance of rain estimated through the following budget calculation:

$$\delta D_{\text{rec}} = \left(\frac{C_D + A_D + E_D}{C_H + A_H + E_H} - 1 \right) \times 1000, \tag{8}$$

where C_D, A_D, and E_D are, respectively, the mass fraction of deuterium in precipitation due to vertical convergence, horizontal advection, and surface evaporation, and C_H, A_H, and E_H are the same for water vapor. At a qualitative level, the comparison between the two leftmost panels of Figure 11 is satisfactory. Having established this, we can try and assess the importance of horizontal and vertical advection in determining the different isotopic composition of rain in the two parts of the basin. In order to do this, we recompute δD_{rec} as indicated by equation (8), but replacing A_D, E_D, A_H, and E_H with their average values computed over both rectangles considered here. The results, shown in the third panel from the left in Figure 11, suggest that, in spite of some differences in the absolute values of δD_{rec}, precipitation in the western part of the Pacific remains more depleted than in the eastern part. Next, we computed δD_{rec} again, this time substituting C_D and C_H with their average values over the two regions of the ocean. The results are represented in the rightmost panel

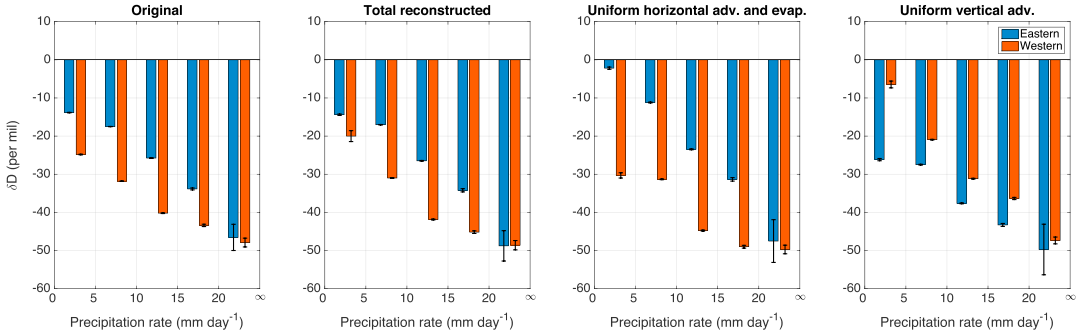

Figure 11. From left to right, δD in precipitation in Western (orange) and Eastern (blue) Pacific diagnosed from iCAM5; δD_{rec} reconstructed using equation (8); δD_{rec} obtained assuming uniform horizontal advection and surface evaporation across the tropical Pacific; δD_{rec} obtained assuming uniform vertical advection in the West and East Pacific.

of Figure 11, and they show that assuming vertical advection to be uniform across the Pacific has a great impact on the isotopic composition of precipitation, making rain in the east even more depleted than the West Pacific. Although this result was obtained from a numerical model, it nevertheless strengthens our conclusion that the differences observed in Figure 10 are mainly to be ascribed to the profiles of vertical velocity being different in the two regions of the tropical Pacific.

Finally, we want to stress again that we do not intend Figure 10 to be taken as the final evidence, the so-called smoking gun, that would put an end to the debate partially reconstructed in section 1. In fact, we recognize that the data that we are using in this section is rather scarce to draw definitive conclusions regarding convection over the Pacific Ocean. Rather, we present this both as a consistency check with the idea of a more bottom heavy vertical velocity in the East compared to the West Pacific and, most importantly, as a preview of the extent to which stable water isotopes could help in understanding convection over the tropical oceans if sufficient data were available.

5. Conclusions

In this manuscript, we have considered the study of convection over the tropical oceans, proposing the use of stable water isotopes to distinguish between different shapes of large-scale vertical velocity: because the vertical profile of the abundance of heavy isotopes tends to be decreasing with height, precipitation generated by convergence of water vapor over a deeper atmospheric layer should be more depleted than it would be if convergence were over a much shallower layer.

To substantiate this thesis, we have first defined two indices: one, given by the ratio of vertically converged over surface evaporated water vapor, C/E, that measures the intensity of convection; the other index is a measure of bottom heaviness of vertical velocity profiles and is defined as the pressure velocity-weighted average pressure, p_ω. With these metrics, we have used a combination of data from GNIP stations and ERA-40 reanalysis to group monthly means of observed δD in precipitation according to the indices defined above. Although noisy, the results show that, for a given value of C/E, precipitation tends to be more depleted when it is associated with more top heavy velocity profiles.

In order to support the validity of these results, we have then provided a number of checks. To begin with, we have verified the significance of the dependence of δD on C/E and p_ω, first by creating 10,000 bootstrap samples from the original data set, and then by doing a bilinear interpolation on each of them. The distribution of coefficients thus obtained shows that the claimed dependence of δD is significant.

Then, we provided a consistency check using a simple model for the isotopic abundance that neglects the contribution from horizontal advection. From a budget perspective, this amounts to saying that precipitation is given by the sum of vertically converged water vapor and the water vapor obtained through surface latent heat fluxes. Using the isotope data derived from IsoSAM and the vertical velocity profiles from ERA-40 reanalysis, we showed that bottom heavy profiles were again associated with more enriched precipitation for a given C/E ratio.

The results from IsoSAM, however, presented a large bias compared to the GNIP data. In order to inspect whether this bias could be ascribed to horizontal advection, we considered a more complex approach and analyzed data from iCAM5, an isotope-enabled GCM. Sampling all the grid points over the tropical oceans and repeating similar analyses to the ones carried out above confirmed the findings implied by the GNIP data set and also that the bias between those and IsoSAM is essentially due to neglecting horizontal advection.

Finally, we speculated on how the results from this manuscript could be used to understand the character of vertical velocity profiles over the tropical Pacific. We sampled a subgroup of GNIP stations, choosing only those in the Pacific Ocean and far from continental areas. We separated the ocean in two regions, west and east, and for every station in each region, we recorded monthly averages of precipitation rates and δD in precipitation. Comparing the abundances of deuterium for a given rain rate across the two areas of the basin shows that precipitation in the West Pacific tends to be more depleted than in the east, except at the highest rain rates. In the light of the main results of this work, we interpret this as a consequence of vertical velocity profiles being more bottom heavy in the latter region. However, we caution the reader against taking this conclusion as carved in stone, particularly as the GNIP stations in the area we have defined as East Pacific do not sample the Intertropical Convergence Zone (ITCZ)—where the majority of deep convection takes place—very well in that part of the basin. For example, the northernmost station in the eastern Pacific is on Christmas Island,

approximately 2° north of the equator. The position of this island suggests that the station samples the ITCZ during spring but that it is too far south during other seasons. Finally, although the scarcity of GNIP data does not allow for a definitive answer, we wish our speculations to motivate the improvement of stable water isotope measurements in the East Pacific, and to inspire further work to place more stringent constraints on large-scale velocity profiles over that area of the globe.

Acknowledgments
The authors thank Peter Blossey, Jesse Nusbaumer, and Martin Singh for their assistance in configuring iCAM5. This work was supported by the NASA grant NNX13AN47 and Harvard Global Institute. The GNIP data used in this manuscript is freely available at http://www.iaea.org/water. The ERA-40 reanalysis data can be obtained from the European Centre for Medium-Range Weather Forecasts. The data and the input files to reproduce the simulations conducted with IsoSAM and iCAM5 are available from the authors upon request.

References

Aggarwal, P. K., O. Alduchov, L. Araguás Araguás, S. Dogramaci, G. Katzlberger, K. Kriz, K. M. Kulkarni, T. Kurttas, B. D. Newman, and A. Purcher (2007), New capabilities for studies using isotopes in the water cycle, *Eos Trans. AGU*, *88*(49), 537–538, doi:10.1029/2007EO490002.

Aggarwal, P. K., U. Romatschke, L. Araguas-Araguas, D. Belachew, F. J. Longstaffe, P. Berg, C. Schumacher, and A. Funk (2016), Proportions of convective and stratiform precipitation revealed in water isotope ratios, *Nat. Geosci.*, *9*(8), 624–629.

Back, L. E., and C. S. Bretherton (2006), Geographic variability in the export of moist static energy and vertical motion profiles in the tropical Pacific, *Geophys. Res. Lett.*, *33*, L17810, doi:10.1029/2006GL026672.

Bailey, A., J. Nusbaumer, and D. Noone (2015), Precipitation efficiency derived from isotope ratios in water vapor distinguishes dynamical and microphysical influences on subtropical atmospheric constituents, *J. Geophys. Res. Atmos.*, *120*, 9119–9137, doi:10.1002/2015JD023403.

Blossey, P. N., Z. Kuang, and D. M. Romps (2010), Isotopic composition of water in the tropical tropopause layer in cloud-resolving simulations of an idealized tropical circulation, *J. Geophys. Res.*, *115*, D24309, doi:10.1029/2010JD014554.

Bony, S., C. Risi, and F. Vimeux (2008), Influence of convective processes on the isotopic composition (δ^{18}O and δD) of precipitation and water vapor in the tropics: 1. Radiative-convective equilibrium and tropical ocean-global atmosphere-coupled ocean-atmosphere response experiment (toga-coare) simulations, *J. Geophys. Res.*, *113*, D19305, doi:10.1029/2008JD009942.

Bosilovich, M. G., J. Chen, F. R. Robertson, and R. F. Adler (2008), Evaluation of global precipitation in reanalyses, *J. Appl. Meteorol. Climatol.*, *47*(9), 2279–2299, doi:10.1175/2008JAMC1921.1.

Cronin, M. F., N. Bond, C. Fairall, J. Hare, M. J. McPhaden, and R. A. Weller (2002), Enhanced oceanic and atmospheric monitoring underway in eastern Pacific, *Eos Trans. AGU*, *83*(19), 205–211, doi:10.1029/2002EO000137.

Dansgaard, W. (1953), The abundance of O^{18} in atmospheric water and water vapour, *Tellus*, *5*(4), 461–469, doi:10.1111/j.2153-3490.1953.tb01076.x.

Dansgaard, W. (1964), Stable isotopes in precipitation, *Tellus*, *16*(4), 436–468, doi:10.1111/j.2153-3490.1964.tb00181.x.

Gedzelman, S. D., and R. Arnold (1994), Modeling the isotopic composition of precipitation, *J. Geophys. Res.*, *99*(D5), 10,455–10,471, doi:10.1029/93JD03518.

Gedzelman, S. D., and J. R. Lawrence (1982), The isotopic composition of cyclonic precipitation, *J. Appl. Meteorol.*, *21*(10), 1385–1404, doi:10.1175/1520-0450(1982)021<1385:TICOCP>2.0.CO;2.

Hartmann, D. L., H. H. Hendon, and R. A. Houze Jr. (1984), Some implications of the mesoscale circulations in tropical cloud clusters for large-scale dynamics and climate, *J. Atmos. Sci.*, *41*(1), 113–121, doi:10.1175/1520-0469(1984)041<0113:SIOTMC>2.0.CO;2.

Hastenrath, S. (2002), The intertropical convergence zone of the eastern Pacific revisited, *Int. J. Climatol.*, *22*(3), 347–356, doi:10.1002/joc.739.

Hendon, H. H., and D. L. Hartmann (1982), Stationary waves on a sphere: Sensitivity to thermal feedback, *J. Atmos. Sci.*, *39*(9), 1906–1920, doi:10.1175/1520-0469(1982)039<1906:SWOASS>2.0.CO;2.

Houze, R. A. (1982), Cloud clusters and large-scale vertical motions in the tropics, *J. Meteorol. Soc. Jpn. Ser. II*, *60*(1), 396–410.

Huaman, L., and K. Takahashi (2016), The vertical structure of the eastern Pacific ITCZs and associated circulation using the trmm precipitation radar and in situ data, *Geophys. Res. Lett.*, *43*, 8230–8239, doi:10.1002/2016GL068835.

Hurrell, J. W., et al. (2013), The community earth system model: A framework for collaborative research, *Bull. Am. Meteorol. Soc.*, *94*(9), 1339–1360, doi:10.1175/BAMS-D-12-00121.1.

Jouzel, J., and L. Merlivat (1984), Deuterium and oxygen 18 in precipitation: Modeling of the isotopic effects during snow formation, *J. Geophys. Res.*, *89*(D7), 11,749–11,757, doi:10.1029/JD089iD07p11749.

Kaye, J. A. (1987), Mechanisms and observations for isotope fractionation of molecular species in planetary atmospheres, *Rev. Geophys.*, *25*(8), 1609–1658, doi:10.1029/RG025i008p01609.

Khairoutdinov, M. F., and D. A. Randall (2003), Cloud resolving modeling of the ARM summer 1997 IOP: Model formulation, results, uncertainties, and sensitivities, *J. Atmos. Sci.*, *60*(4), 607–625, doi:10.1175/1520-0469(2003)060<0607:CRMOTA>2.0.CO;2.

Konecky, B., D. Noone, J. Nusbaumer, and K. Cobb (2014), Enso and Indo-Pacific water isotopes: Observations, modeling, and implications for proxy reconstructions, Abstracts PP31D-1169 presented at 2014 Fall Meeting, AGU, San Francisco, Calif., 14–18 Dec.

Kurita, N., D. Noone, C. Risi, G. A. Schmidt, H. Yamada, and K. Yoneyama (2011), Intraseasonal isotopic variation associated with the Madden-Julian oscillation, *J. Geophys. Res.*, *116*, D24101, doi:10.1029/2010JD015209.

Lebsock, M. D., and T. S. L'Ecuyer (2011), The retrieval of warm rain from cloudsat, *J. Geophys. Res.*, *116*, D20209, doi:10.1029/2011JD016076.

Lee, J.-E., I. Fung, D. J. DePaolo, and C. C. Henning (2007), Analysis of the global distribution of water isotopes using the NCAR atmospheric general circulation model, *J. Geophys. Res.*, *112*, D16306, doi:10.1029/2006JD007657.

LeGrande, A. N., and G. A. Schmidt (2006), Global gridded data set of the oxygen isotopic composition in seawater, *Geophys. Res. Lett.*, *33*, L12604, doi:10.1029/2006GL026011.

Lin, Y.-L., R. D. Farley, and H. D. Orville (1983), Bulk parameterization of the snow field in a cloud model, *J. Clim. Appl. Meteorol.*, *22*(6), 1065–1092, doi:10.1175/1520-0450(1983)022<1065:BPOTSF>2.0.CO;2.

Liu, C., S. Shige, Y. N. Takayabu, and E. Zipser (2015), Latent heating contribution from precipitation systems with different sizes, depths, and intensities in the tropics, *J. Clim.*, *28*(1), 186–203, doi:10.1175/JCLI-D-14-00370.1.

Liu, Z., D. Ostrenga, W. Teng, and S. Kempler (2012), Tropical rainfall measuring mission (TRMM) precipitation data and services for research and applications, *Bull. Am. Meteorol. Soc.*, *93*(9), 1317–1325, doi:10.1175/BAMS-D-11-00152.1.

Mears, C. A., and F. J. Wentz (2005), The effect of diurnal correction on satellite-derived lower tropospheric temperature, *Science*, *309*(5740), 1548–1551, doi:10.1126/science.1114772.

Mitas, C. M., and A. Clement (2006), Recent behavior of the Hadley cell and tropical thermodynamics in climate models and reanalyses, *Geophys. Res. Lett.*, *33*, L01810, doi:10.1029/2005GL024406.

Moore, M., Z. Kuang, and P. N. Blossey (2014), A moisture budget perspective of the amount effect, *Geophys. Res. Lett.*, *41*, 1329–1335, doi:10.1002/2013GL058302.

Moore, M., P. N. Blossey, A. Muhlbauer, and Z. Kuang (2016), Microphysical controls on the isotopic composition of wintertime orographic precipitation, *J. Geophys. Res. Atmos.*, *121*, 7235–7253, doi:10.1002/2015JD023763.

Neale, R. B., et al. (2010), Description of the NCAR community atmosphere model (CAM 5.0), Natl. Cent. For Atmos. Res., Boulder, Colo.

Nusbaumer, J. (2016), An examination of atmospheric river moisture transport and hydrology using isotope-enabled CAM5, PhD thesis, Univ. of Colorado, Boulder, Colo.

Nusbaumer, J., T. Wong, and D. Noone (2014), The impact of differing land surface models and water isotopic parameterizations to the distribution of water isotopes in a coupled atmosphere-land global climate model. Abstract PP33F-04 presented at 2014 Fall Meeting, AGU, San Francisco, Calif., 9–13 Dec.

O'Brien, T. A., W. D. Collins, K. Kashinath, O. Rübel, S. Byna, J. Gu, H. Krishnan, and P. A. Ullrich (2016), Resolution dependence of precipitation statistical fidelity in hindcast simulations, *J. Adv. Model. Earth Syst.*, *8*, 976–990, doi:10.1002/2016MS000671.

Raymond, D. J., S. K. Esbensen, C. Paulson, M. Gregg, C. S. Bretherton, W. A. Petersen, R. Cifelli, L. K. Shay, C. Ohlmann, and P. Zuidema (2004), Epic2001 and the coupled ocean–atmosphere system of the tropical East Pacific, *Bull. Am. Meteorol. Soc.*, *85*(9), 1341–1354, doi:10.1175/BAMS-85-9-1341.

Risi, C., S. Bony, and F. Vimeux (2008), Influence of convective processes on the isotopic composition (δ^{18}O and δD) of precipitation and water vapor in the tropics: 2. Physical interpretation of the amount effect, *J. Geophys. Res.*, *113*, D19306, doi:10.1029/2008JD009943.

Rozanski, K., L. Araguás-Araguás, and R. Gonfiantini (1993), Isotopic patterns in modern global precipitation, in *Climate Change in Continental Isotopic Records*, edited by P. K. Swart et al., pp. 1–36, AGU, Washington, D. C., doi:10.1029/GM078p0001.

Santer, B. D., J. J. Hnilo, T. M. L. Wigley, J. S. Boyle, C. Doutriaux, M. Fiorino, D. E. Parker, and K. E. Taylor (1999), Uncertainties in observationally based estimates of temperature change in the free atmosphere, *J. Geophys. Res.*, *104*(D6), 6305–6333, doi:10.1029/1998JD200096.

Santer, B. D., et al. (2005), Amplification of surface temperature trends and variability in the tropical atmosphere, *Science*, *309*(5740), 1551–1556, doi:10.1126/science.1114867.

Schotter, U., F. Oldfield, and K. Froehlich (1996), *Gnip. Global Network for Isotopes in Precipitation*, Laederach AG, Bern, Switz.

Schumacher, C. R. A. H., Jr., and I. Kraucunas (2004), The tropical dynamical response to latent heating estimates derived from the TRMM precipitation radar, *J. Atmos. Sci.*, *61*(12), 1341–1358, doi:10.1175/1520-0469(2004)061<1341:TTDRTL>2.0.CO;2.

Sherwood, S. C., J. R. Lanzante, and C. L. Meyer (2005), Radiosonde daytime biases and late-20th century warming, *Science*, *309*(5740), 1556–1559, doi:10.1126/science.1115640.

Simmons, A., and J. Gibson, (2000), The ERA-40 project plan, ERA-40 Project Rep. Ser. No. 1, 63 pp., ECMWF, Reading, U. K.

Simpson, J., R. F. Adler, and G. R. North (1988), A proposed tropical rainfall measuring mission (TRMM) satellite, *Bull. Am. Meteorol. Soc.*, *69*(3), 278–295, doi:10.1175/1520-0477(1988)069<0278:APTRMM>2.0.CO;2.

Trenberth, K. E., D. P. Stepaniak, and J. M. Caron (2000), The global monsoon as seen through the divergent atmospheric circulation, *J. Clim.*, *13*(22), 3969–3993, doi:10.1175/1520-0442(2000)013<3969:TGMAST>2.0.CO;2.

White, J. W. C., and S. D. Gedzelman (1984), The isotopic composition of atmospheric water vapor and the concurrent meteorological conditions, *J. Geophys. Res.*, *89*(D3), 4937–4939, doi:10.1029/JD089iD03p04937.

Zhang, C., M. McGauley, and N. A. Bond (2004), Shallow meridional circulation in the tropical eastern Pacific, *J. Clim.*, *17*(1), 133–139, doi:10.1175/1520-0442(2004)017<0133:SMCITT>2.0.CO;2.